J. Fluid Mech. (1983), *vol.* 126, *pp.* 443–461
Printed in Great Britain

High-strain-rate free-surface boundary-layer flows

By J. R. BERTSCHY,† R. W. CHIN‡ AND F. H. ABERNATHY
Harvard University, Division of Applied Sciences, Cambridge, Massachusetts 02138

(Received 28 January 1981 and in revised form 11 November 1981)

Two-dimensional boundary-layer flows of water down an inclined table were investigated in both the laminar and turbulent regimes. Mean, r.m.s. and skewness and velocity spectra were determined from streamwise velocity measurements. Two laser-Doppler anemometry methods were developed (for studying polymer-solution flows using this same water table) and compared with measurements obtained using hot-film anemometry. All three techniques obtained consistent results.

An analysis based on a von Mises transformation is presented which accurately predicts the mean-velocity profile and flow development in the laminar regime. High strain rates are achieved which can be varied independently of Reynolds number, and turbulent flows are easily generated by inserting a disturbance. These turbulent flows are surprisingly similar to more commonly investigated turbulent boundary-layer flows of much greater y^+ extent. Turbulent water-table flows typically extend only to $y^+ = 100$, yet mean velocity essentially follows the law of the wall, and intensity and skewness measurements are similar to those obtained in flows much less limited in y^+.

1. Introduction

One way to increase understanding of mixing processes in turbulent boundary layers would be to compare pure-water flows with those of dilute drag-reducing polymer solutions in an identical geometry. This task is not straightforward because of instrumentation difficulties associated with polymer-solution flows and because of the high strain rates necessary to achieve turbulent drag reduction. For example, a commonly studied drag-reducing agent such as polyethylene oxide WSR-301 requires a strain rate of the order of 1000 s^{-1} to be effective. Only laser-Doppler anemometry (LDA) provides reliable velocimetry in polymer-solution flows, and adequate spatial resolution becomes difficult if not impossible to obtain in the small-diameter tubes conventionally used to achieve the high strain rates. When this study was initiated, there was also speculation that the addition of polymers caused transition to turbulence at lower Reynolds numbers than observed in Newtonian fluid flows (Hansen *et al.* 1974; Jones, Marshall & Walker 1976). This suggested the need for stability studies of laminar flows of polymer solutions.

To pursue such an investigation, a well-documented two-dimensional high-strain-rate flow was required which could be maintained as either laminar or turbulent with unambiguous indications of the flow condition. Additionally, it was thought important to be able to keep the Reynolds number of the flow fixed, yet adjust the strain rate,

† Present address: IBM, G.P.D. Lab., Dept F-44005, 5600 Cottle Road, San José, California 95193.

‡ Present address: Shell Development Company, Westhollow Research Center E-1340, P.O. Box 1380, Houston, Texas 77001.

thereby varying the polymer activity. No flow fulfilled all of these requirements; however, the free-surface flow down a water table nearly did so. It only lacked detailed documentation for pure-water flows. This paper provides such documentations in both the laminar and turbulent regimes. In addition, the adequacy of two novel LDA techniques developed for polymer studies is verified by comparison with results obtained using standard hot-film instrumentation in water flows where all three techniques are reliable.

Section 2 describes the flow apparatus and its capabilities in detail; §3 presents a model for the laminar flow and establishes its validity by comparison to experiment; §4 describes the velocimetry and experimental procedures; and §5 documents the turbulent flow of the water table in the form of mean, r.m.s. and skewness velocities, and spectra.

These measurements of turbulent flows on the water table should be of intrinsic interest to those concerned with the relative importance of the inner and outer flows of a turbulent boundary layer. The extent of the outer flow can be decreased by increasing the table inclination at a fixed mass flow.

2. Description of the flow facility

The essential physical arrangements of the water-table flow facility are sketched in figure 1. Details of the water filtration, constant-flow-rate supply and weighing procedures are contained in Bertschy & Abernathy (1977) or Bertschy (1979). Filtered water is supplied at a constant, but adjustable, rate to the water table on the left as shown. Various devices are used to decrease the amplitude of surface waves, and to ensure uniformity of the flow in the settling chamber. The flow proceeds through a free-surface contraction and down the table, which is at a fixed, though adjustable, inclination of up to 5° from the horizontal. The flow can then be collected in a weighing tank for mass-flow measurements. Some general features of the inclined water channel or table are worth mentioning. The inlet and working section (a 4 ft wide by 6 ft long sheet of glass, $\frac{1}{2}$ in. thick, with glass sidewalls), together form a rigid unit which can be pivoted about the fixed upstream support by adjusting the elevation of the downstream support (figure 1). Typical depths for a high-strain-rate flow (large inclination) are 2–3 mm. Because the span of the working section is at least two orders of magnitude larger than the flow depth, it is realistic to consider the flow near the centre to be two-dimensional.

With the well-designed inlet section, the flow on the water table is laminar if left undisturbed, and the free surface is mirror-like. Provided that the Reynolds number Re (based on local mean velocity and depth) is below 5000, laminar flow can be maintained throughout the working section. Continuity requires the product of local mean velocity and depth to be a constant for a given flow state. Hence, this Reynolds number is also constant and independent of both distance downstream and the inclination of the table. The wall strain rate (or inclination) and Reynolds number are therefore independent variables.

Turbulent flow on the table is achieved by placing a trip spanwise to the flow. Spot transition is easily obtained by generating a local upstream disturbance. Figure 2 is a photograph of a turbulent spot imbedded in a laminar flow. The free surface over the spot is corrugated in a random time-dependent manner in response to the turbulent pressure fluctuations beneath it. This effortless flow-visualization feature made it possible to distinguish clearly between fluctuations in laminar polymer flows and turbulence (Abernathy *et al.* 1980). While water-table flows have been used in

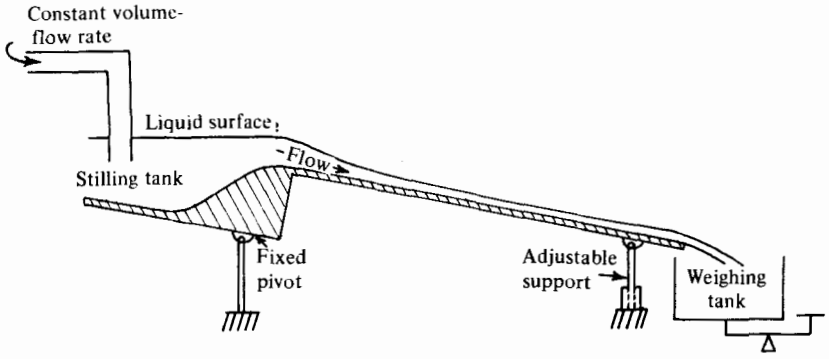

FIGURE 1. Schematic side view of the water table.

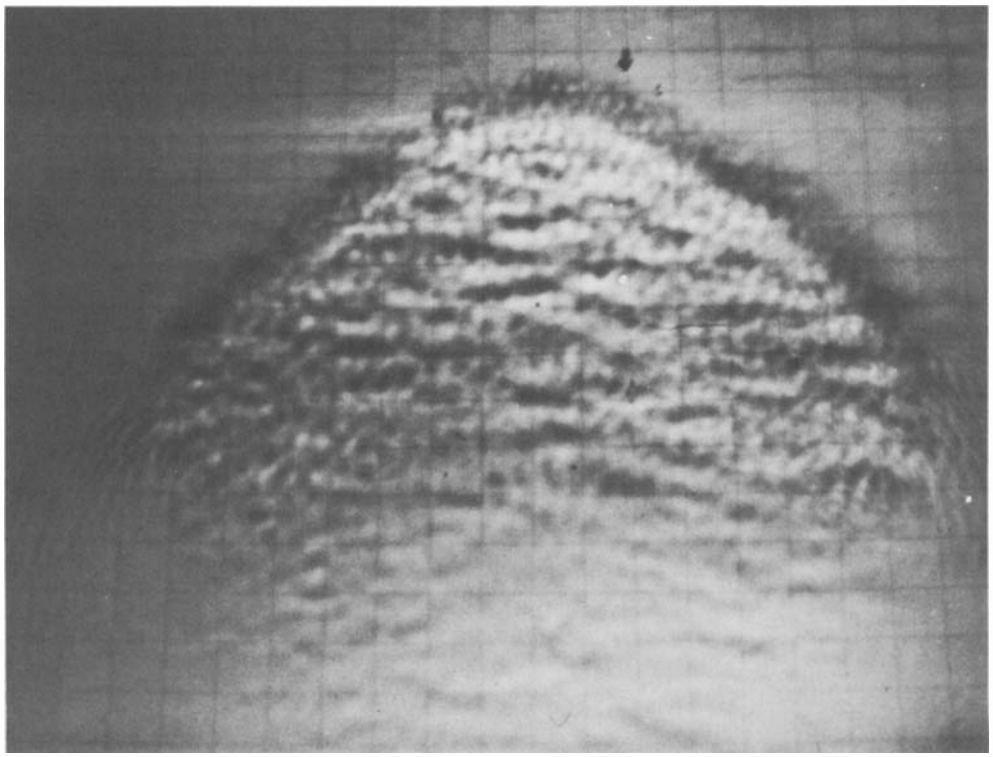

FIGURE 2. Photograph of the free surface over an isolated turbulent spot. The flow is from top to bottom.

research before, for example Emmons' (1951) pioneering work on turbulent spots, neither the laminar nor turbulent flows have been carefully studied and reported in the literature.

3. Description of the laminar flow

The steady laminar flow of an incompressible Newtonian fluid (pure water) on the water table is determined by the volume flow rate, inclination angle, and distance downstream from a given initial velocity profile. The flow geometry and defining

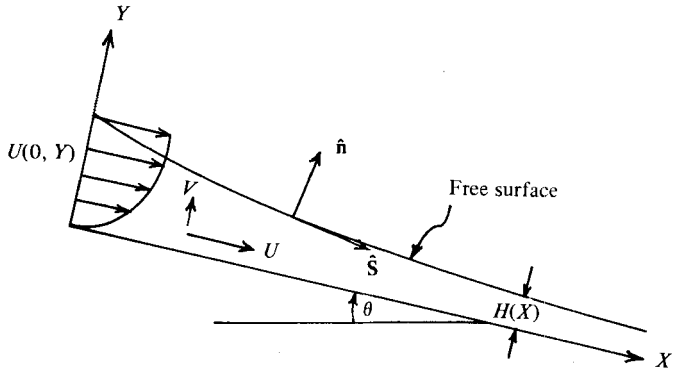

FIGURE 3. Schematic side view of the water-table flow indicating the variable definitions.

variables are shown schematically in figure 3. At large X, the flow approaches an asymptotic condition where the velocity profile varies parabolically in Y:

$$U(\infty, Y) \equiv \frac{g}{\nu} \sin\theta [H_\infty Y - \tfrac{1}{2} Y^2], \tag{1}$$

where g is the gravitational force per unit mass, ν is the kinematic viscosity and H_∞ is the asymptotic flow depth. This depth is determined by the volume flow rate per unit span of flow Q, or

$$H_\infty = \left(\frac{3\nu Q}{g \sin\theta}\right)^{\frac{1}{3}}. \tag{2}$$

The asymptotic mean velocity $\bar{U} = Q/H_\infty$ and H_∞ will be used as the characteristic velocity and length to form the dimensionless parameters for the calculations.

The dimensional constant-viscosity momentum and continuity equations (using index notation) are respectively

$$U_j U_{i,j} = -\frac{1}{\rho} P_{,i} + g_i + \nu U_{i,jj}, \tag{3}$$

$$U_{i,i} = 0, \tag{4}$$

where P is the pressure and ρ the fluid density; U_i and g_i are the velocity and gravitational components in the ith direction, with $i = 1$ being the streamwise coordinate X ($U_1 \equiv U$ and $g_1 \equiv g \sin\theta$) and $i = 2$ being the normal component Y ($U_2 \equiv V$ and $g_2 \equiv -g \cos\theta$).

Dimensional velocities, coordinates and pressure will be denoted by capital letters, leaving lower-case letters for dimensionless forms. A comma after a variable indicates differentiation with respect to the subscripted variable. Summation on repeated indices occurs only for the indices i and j.

The equations of motion hold between $y = 0$, the glass bottom of the water table, and $Y = H$, the free surface. The location of the free surface at $X = 0$ must be given as part of the initial velocity profile and is known asymptotically; it must be determined for finite values of X.

The boundary conditions at the solid surface are

$$U_i = 0 \quad \text{at} \quad Y = 0, \quad X > 0. \tag{5a}$$

At the free surface, surface tension σ should be considered, and the conditions of the air above the water specified. As a simplification the air was assumed to have zero

inertia compared to that of the flow. With σ constant, these assumptions lead to the condition that the tangential component of the stress at the free surface must be zero. The normal component of the stress must balance the surface-tension stress σ/R, where R is the radius of curvature. These stress conditions are, using the unit normal component n_i and unit tangent component s_i,

$$\text{normal } \tau_{ij} n_i n_j = \sigma/R, \tag{5b}$$

$$\text{tangent } \tau_{ij} n_i s_j = 0 \tag{5c}$$

at $Y = H(X)$, $X > 0$, where the stress tensor is $\tau_{ij} = -P\delta_{ij} + \mu(U_{i,j} + U_{j,i})$, and μ is the molecular viscosity.

For the flows of interest, where $Re \gg 1$, the standard boundary-layer assumptions ($U_{,YY} \gg U_{,XX}$ and $H(X) \ll X$) reduce the complexity of (3) and (4), and in dimensionless form they become

$$uu_{,x} + vu_{,y} = -p_{,x} + 3 + u_{,yy}, \tag{6}$$

$$p_{,y} = -\frac{gH_\infty}{\bar{U}^2}\cos\theta, \tag{7}$$

$$u_{,x} + v_{,y} = 0, \tag{8}$$

using the following definitions:

$$Re \equiv \frac{\bar{U}H_\infty}{\nu} = \frac{Q}{\nu}, \quad x \equiv \frac{X}{Re\, H_\infty}, \quad y \equiv \frac{Y}{H_\infty}$$

$$u(x,y) = u \equiv \frac{U}{\bar{U}}, \quad v(x,y) = v \equiv \frac{V\, Re}{\bar{U}}, \quad p \equiv \frac{P}{\rho\bar{U}^2}.$$

The no-slip boundary conditions (5a) expressed non-dimensionally are

$$u = v = 0 \quad \text{at} \quad y = 0, \quad x > 0,$$

while the stress conditions (5b, c) must hold at the free surface $y = h(x) \equiv H(X)/H_\infty$. The normal stress condition (5b) leads to the following dimensionless relation for the pressure, after dropping terms in $(h_{,x})^2$ compared with unity,

$$p = -\frac{2}{Re^2}u_{,x} - \frac{2}{Re^2}u_{,y}h_{,x} - \frac{2}{Re^4}uh_{,x}h_{,xx} - \frac{1}{We^2Re^2}h_{,xx} \quad \text{at} \quad y = h(x), \tag{9}$$

where the Weber number $We \equiv \bar{U}/(\sigma/\rho H_\infty)^{\frac{1}{2}}$. Unless the Weber number is very much less than one, the dimensionless pressure at the free surface is of the order of Re^{-2}. The Weber number is in fact of order unity for water and the dilute polymer flows of interest. The slope $h_{,x}$ of the free surface is of order unity except near $x = 0$, and even here for the flows to be investigated $h_{,x}$ and $h_{,xx}$ are nearly unity. Taking the pressure to be zero at the free surface implies neglecting terms of the same order as the neglected horizontal diffusion terms. Hence the equation

$$p(x, h(x)) = 0 \tag{10a}$$

is consistent with the boundary-layer approximations. The shear-stress boundary condition (5c) expressed non-dimensionally is

$$u^2u_{,y} + \frac{1}{Re^2}\left(u^2v_{,x} - 4uu_{,x}v - v^2u_{,y} - \frac{1}{Re^2}v^2v_{,x}\right) = 0 \quad \text{at} \quad y = h(x). \tag{10b}$$

It is clear that $u_{,y} = 0$ is consistent with the boundary-layer assumptions; however, since it causes no difficulty, the entire equation (10*b*) will be retained in the calculations.

A similarity solution of the equations of motion does not exist, so one must resort to either approximate solutions or numerical integration. The primary difficulty in either approach is that the location of the free surface is unknown, although it is a streamline of the flow. This suggests that a von Mises (1927) transformation of the independent variables would be useful. The new coordinates (ξ, ψ) form a non-orthogonal set and are defined as

$$\xi \equiv x, \quad \psi(x, y) = \int_0^y u(x, z)\, dz. \tag{11}$$

Using continuity, the two momentum equations become

$$\tfrac{1}{2}(u^2)_{,\xi} = -p_{,\xi} + vp_{,\psi} + 3 + \tfrac{1}{2}u(u^2)_{,\psi\psi}, \tag{12}$$

$$up_{,\psi} = -\frac{gH_\infty}{\bar{U}^2}\cos\theta. \tag{13}$$

In this coordinate system the flow is between $\psi = 0$ and $\psi = 1$. Pressure can be eliminated from (12) by integrating the hydrostatic approximation along with the boundary condition (10*a*). The resulting equation to be integrated is then

$$[\phi + 2ch(\xi)]_{,\xi} = 6 + \phi^{\frac{1}{2}}\phi_{,\psi\psi}, \tag{14}$$

where

$$\phi \equiv u^2(\xi, \psi), \quad c = \frac{gH_\infty \cos\theta}{\bar{U}^2}.$$

The boundary conditions are $\phi(\psi = 0) = 0$ and the zero-shear-stress condition (10*b*) at $\psi = 1$. This latter boundary condition expressed in the transformed coordinates is

$$\tfrac{1}{2}\phi_{,\psi}[Re^2 + (h_{,\xi})^2]^{\frac{1}{2}}\phi^{\frac{1}{2}} - h_{,\xi}[Re^2 + (h_{,\xi})^2]\phi_{,\xi} + h_{,\xi\xi}[Re^2 - (h_{,\xi})^2]\phi = 0. \tag{15}$$

In order to perform the numerical integration of (14), one must specify a profile at $x = 0$, the entrance to the water table. This initial condition is determined by the physical requirement that the flow is critical (Froude number = 1) at some point where the bottom surface reaches a maximum elevation. If one assumes that the velocity profile is uniform, then $U(0, Y) = (gH(0))^{\frac{1}{2}}$ and $H(0) = (Q^2/g)^{\frac{1}{3}}$. For other profiles the critical condition can be calculated by considering the limiting case for an infinitesimal hydraulic jump. The calculated initial depth for different assumed profiles increases with the departure from uniformity; it is 6 % larger for a parabolic profile and 10 % larger for a linear one. The calculated free-surface velocity naturally increases to conserve the volume flux. The calculated variation of $H(X)$ (figure 4) is relatively insensitive to the assumed initial velocity profile beyond $X = 40$ cm.

The equation of motion (14) with its boundary conditions constitutes an initial-value problem (with ξ and ψ as coordinates) which was solved by standard numerical integration techniques. Transforming this solution to the physical coordinates X and Y involved a combination of an analytic expansion about a singularity at the solid surface (Mitchell & Thomson 1958) and numerical integration.

Figure 4 portrays the calculated variation of $H(X)$ for four different assumed initial velocity profiles. The depth (and hence velocity profiles) at each X beyond 80 cm is essentially independent of the choice of initial profile. By comparing calculated and measured depths for $X < 80$ cm it was determined that a uniform initial velocity profile most closely modelled the water-table flows. Other initial

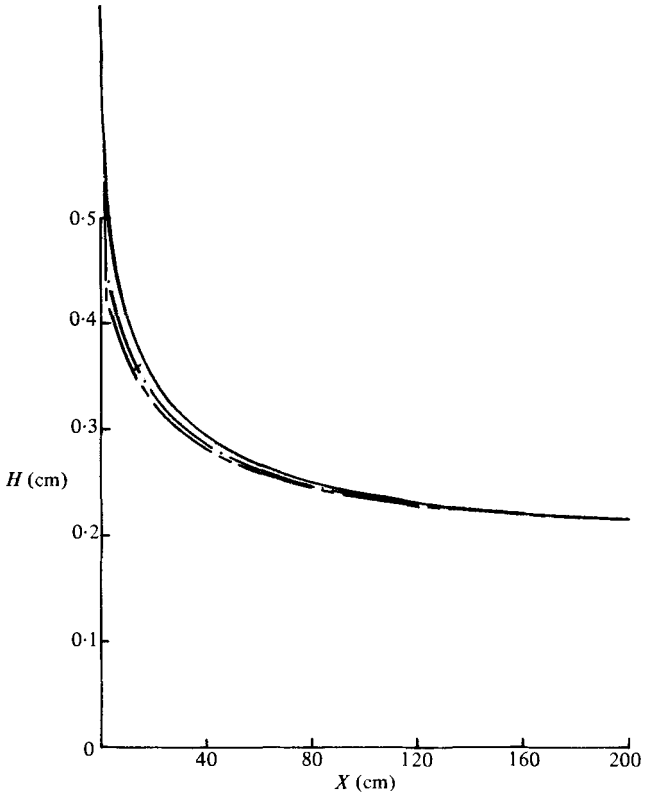

FIGURE 4. The calculated variation in flow depth for the following initial profiles (A and B are constant parameters): ——, $U(0) = \text{const}$; –·–, $U(0) = A \sin(\pi Y/2H(0))$ or AY^2+BY; – – –, $U(0) = AY$.

velocity profiles predict shallower flows than those observed for $X < 80$ cm. Comparisons of the calculated flow depth (based on a uniform initial profile) and measurements are shown in figure 5, and the calculated and measured velocity profiles are presented in figure 6. It is apparent that there is excellent agreement at $X = 10$ cm and beyond. The velocity profile is nearly parabolic beyond 70 cm on the table. The difference between the profiles at 70 and 150 cm in figure 6 is due primarily to the difference in depth between the two locations. A dimensionless profile, using local depth and free-surface velocity as the characteristic scales, would show little change in profile shape beyond 70 cm.

Stability

Lin (1967) studied the linear stability of the asymptotic profile (1); however, an incorrect normal-stress boundary condition was used in the analysis. De Bruin (1974) solved the correctly formulated problem numerically, omitting surface-tension effects. An independent investigation of this stability problem including surface-tension and profile (form-factor) effects was undertaken for the water table. The surface (gravity) mode is found to be moderately stabilized by increasing the surface tension or by decreasing the inclination angle (cf. Yih 1963). Over the range of parameters appropriate for water-table flows, the surface mode is mathematically always unstable, in agreement with de Bruin. No evidence of this instability, however, was found on the water table. To first order, the shear mode is unaffected by changes in surface tension or inclination angle (1–5°). Thus the flow can be

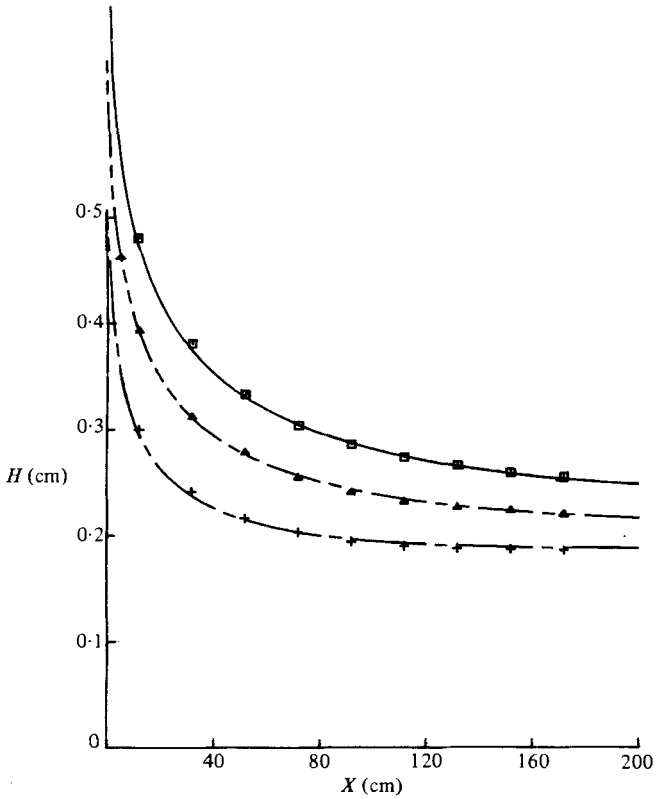

FIGURE 5. A comparison of several calculated and measured laminar-flow depths. The calculations assumed $U(0) = \text{const.}$

Experimental	Calculated	Q (cm²/s)
□	——	21·6
△	– – –	16·4
+	– – – –	11·2

considered to be plane Poiseuille as far as the shear-wave instability is concerned. Form-factor effects, however, are substantial. Profiles near the inlet can easily have a minimum critical Reynolds number of 50000 compared with the 5600 associated with the asymptotic profile. (The topic of stability is complex and interesting in its own right and is therefore deferred to a separate paper.)

4. Velocimetry and experimental procedures

Three different anemometry techniques were used to measure the instantaneous velocity at a point in the flow. A hot-film sensor was used as a standard to which results obtained by two novel laser-Doppler methods (developed primarily for later use with dilute polymer flows) were compared.

The hot-film sensing element was a TSI Model 1218-20W boundary-layer probe (0·002 in. diameter, coated for use in water), which was driven by a TSI Model 1053B constant-temperature bridge circuit. The output voltage was sampled periodically and stored in a computer memory. Each measured voltage was converted to a flow velocity through the use of an experimentally determined calibration relation. A separate water-flow facility was used for the calibration using a standard dual-beam

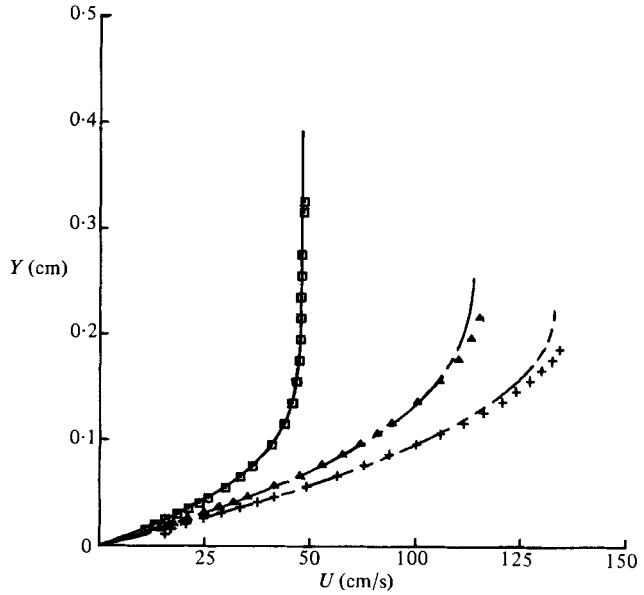

FIGURE 6. A comparison of several calculated and measured laminar velocity profiles for $Q = 16{\cdot}4$ cm^2/s.

Experimental	Calculated	X (cm)
□	——	10
△	– – –	70
+	– · – · –	150

forward-scattering LDA arrangement (Bertschy 1979). The facility used the potential-flow region of the discharge from a 1 in. diameter submerged nozzle. The geometric extent of this region of uniform flow was determined from LDA traverses.

The use of laser-Doppler techniques for velocity measurements normally involves sacrificing good resolution and continuous velocity data in return for the non-intrusive nature of the laser beam. One of the two LDA techniques developed for use with the two-dimensional water-table flow overcame the conventional loss of spatial resolution by selectively seeding the flow with light-scattering agents introduced upstream of the light-scattering volume. The long dimension of the optical volume was fixed normal to the wall, across the gradient of the flow. Bubbles were generated by electrolysis from a fine wire (0·001 in. diameter) positioned transverse to the flow and parallel to the bottom wall, a measured distance away. The sheet of bubbles generated by the wire was convected by the flow, intersecting the optical volume nearly perpendicularly to its long axis. The effective scattering-volume dimensions were the thickness of the bubble sheet in the direction of the gradient and the focusing diameter spanwise to the flow. This volume is nearly comparable to that of the hot-film sensor. Details of the method have been described by Abernathy, Bertschy & Chin (1977).

The major drawback of the selective-seeding technique is that a velocity correction must be applied to account for the wake of the bubble-generating wire, even at 400 wire diameters downstream of the wire (where the LDA velocity measurements were made). Over the velocity range encountered on the water table it has been shown (Abernathy *et al.* 1977) that the wake correction depends only on the dimensionless spacing between the wire and the scattering volume. At a 400-diameter spacing, the true velocity was obtained by multiplying the measured bubble velocity by 1·07, independent of the elevation of the wire in the flow (i.e. independent of wire Re).

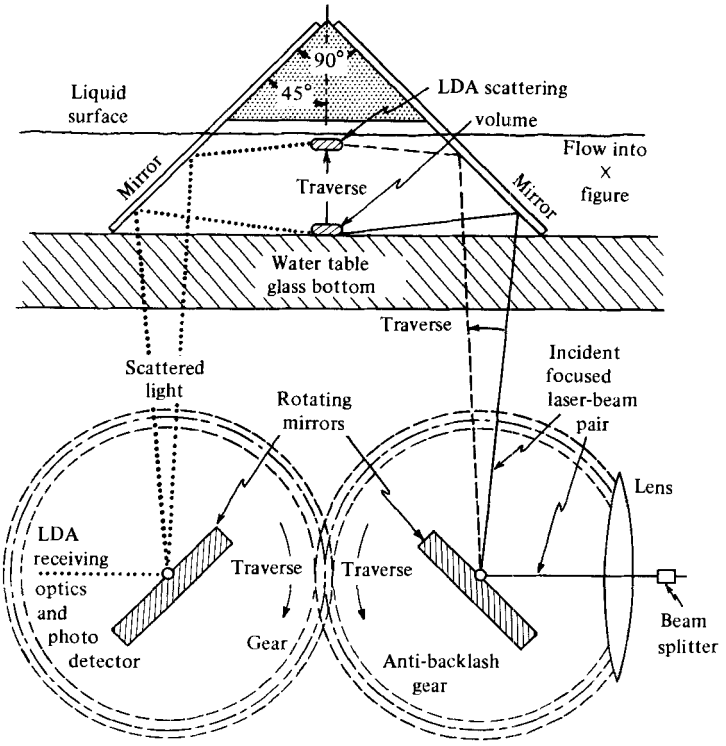

FIGURE 7. Side view (looking downstream) of the optical arrangement used to traverse the LDA scattering volume. The position of the LDA scattering volume (the intersection point of the focused, laser-beam pair) is changed by rotating the mirrors, which are coupled by gears. One mirror (shown on the right) sweeps the scattering volume through a long arc, and the other rotates (in the opposite direction) so that light scattered from particles moving through the scattering volume is directed to the receiving optics.

The other LDA technique used was essentially a variation of a standard, dual-beam forward-scattering optical system. Water-soluble paint at a concentration of $\frac{1}{2}$ p.p.m. was added to the water flow to provide sufficient light-scattering agents (titanium dioxide) throughout the fluid. This technique will be called uniform seeding in contrast with the selective-seeding LDA method. The novel aspect of the uniform-seeding LDA involved the method whereby the optical scattering volume traversed the flow across the velocity gradient (see figure 7). The long axis of the optical volume, about 1·6 mm, is nearly parallel to the wall and transverse to the flow. The spatial resolution was then determined by the scattering-volume diameter of about 0·11 mm. The optical method that enabled the scattering volume to traverse the flow without moving the transmission or receiving lenses is described in Bertschy & Abernathy (1981), along with other experimental features.

Both LDA configurations used TSI 900 series optics (119 mm focal length) and a TSI Model 952 photodiode. A CW Radiation Model LS-16P He–Ne laser (22 mW polarized output) was used throughout. A TSI Model 1090 tracker converted the Doppler signals to voltages proportional to velocity. Because the count rate exceeded 1 kHz, the tracker voltage output was analysed as if it were continuous.

Data analysis was performed on velocity records stored in a PDP 11/10 computer (32K words memory). Each record consisted of 10240 digital conversions of the analogue voltage sampled at a 1 kHz rate. This rate was selected because it

considerably exceeded the highest frequencies found in turbulent water flows generated on the water table. The length of the data record (about 10 s), was sufficiently long because there is very little turbulent energy below 1 Hz. The particular length was selected to facilitate spectral analysis. To obtain spectra 2048 point records were transformed at a time (owing to limited computer memory), and the resultant five transforms were averaged to obtain a single velocity spectrum for a data record.

One difficulty common to all three anemometry techniques was locating the measuring point relative to the wall. The location of different points on the traverse relative to one another was accurately determined by a dial indicator or micrometer, but the reading that corresponded to $Y = 0$ (the wall) was not well-known. If the dial indicator reading is defined as D, the location of the wall was at some unknown reading, say ϵ, such that

$$Y = D - \epsilon.$$

The value of ϵ was determined by fitting a low-order polynomial in the variable $(D-\epsilon)/H$ to laminar mean-velocity profiles using the method of least squares. The polynomials all satisfied the boundary conditions

$$U(Y=0) = 0, \quad \left.\frac{dU}{dY}\right|_{Y=H} = 0.$$

The value of ϵ that gave the best least-squares fit to the data was selected as the location of the wall.

Mean-velocity profiles of laminar flows were essentially parabolic, because the flow had nearly accelerated to the asymptotic form at the measuring station ($X = 150$ cm). Parabolic or cubic polynomials led to excellent fits of the data, with little uncertainty in the wall location. An uncertainty of 0·002 cm was tolerated. Once established for a given anemometry technique by fitting to laminar data, ϵ was assumed to be the same for turbulent flows measured concurrently, and higher-order polynomials provided reasonable descriptions of the mean turbulent-velocity profiles.

After a functional representation of the mean velocity is established, the velocity obtained by anemometry can be compared with independently acquired information. The flow over the water table was monitored using a weighing tank and stopwatch. Together with the density this can be used to obtain a measure of the volume flow rate over the water table Q_v. This can be compared with the integrated velocity profile from an anemometer, the ratio of the two being

$$RQ = \frac{Q_v}{\left(\int_0^H U\,dY\right)(\text{span})}.$$

RQ for the hot-film and uniform-seeding LDA velocity data was always near unity as expected. Owing to the bubble-wire wake, data obtained by selective-seeding LDA led to $RQ \approx 1{\cdot}10$. This is considered to be in reasonable agreement with the correction factor of 1·07 as determined in Abernathy *et al.* (1977), considering the slight deviations from flatness of the glass bottom of the water table.

When using selective-seeding LDA an additional verification was possible. The free-surface velocity was measured directly by sprinkling powder on the surface far upstream of the LDA measuring volume, which was adjusted to intersect the free surface. No electrolysis bubbles were generated; therefore, only the powder produced a Doppler signal. This was sufficient to obtain a reasonable mean-velocity measurement, although the signal density was too low for higher moments or spectra. The

mean-velocity profile as measured by selective seeding could be extrapolated to the surface as a second verification of the correction factor for the bubble-wire wake. Agreement within 5% was considered acceptable.

A standard method of presenting turbulent velocity data is by normalizing with the wall shear velocity u_τ and ν. The wall-friction velocity was determined from depth and mass-flow measurements, and viscosity was determined by monitoring temperature. It would have been possible to find u_τ by extrapolating the mean profile to the wall, since

$$u_\tau = \left(\nu \left.\frac{dU}{dY}\right|_{Y=0}\right)^{\frac{1}{2}},$$

but data near the wall were relatively unreliable, hence such extrapolation could involve unknown errors.

Depth and mass-flow measurements yield a measure of u_τ independent of the anemometry techniques in much the same way that pressure taps are used in pipe flows. A momentum balance of flow acceleration, wall friction, depth change and gravity can be used to determine u_τ. At a measuring station 150 cm down the water table the flow is nearly in equilibrium; gravity and friction nearly balance, hence

$$u_\tau \approx (gH \sin\theta)^{\frac{1}{2}}.$$

The actual computation used incorporated any measurable flow acceleration and is described in Bertschy (1979).

These techniques of measurement and data reduction were used to obtain some of the data already described in §3 and the turbulent boundary-layer measurements in §5.

5. Turbulence measurements

Turbulent flow is achieved on the water table by inserting a trip at the inlet. A beaded chain held spanwise introduces large three-dimensional disturbances to the flow. The free surface of a laminar flow is mirror-like, while that of the corresponding turbulent flow is rippled in time-varying patterns. At a fixed flow rate and table inclination, a turbulent flow is deeper than a laminar one. This increased depth is a result of the higher wall shear stress. Turbulent flows achieve an asymptotic depth within a few centimetres of the trip. Hence there are no mean gradients in the flow direction in the vicinity of the measuring station. While operating below the two-dimensional critical Re (de Bruin 1974), the generated turbulent boundary layer shows no signs of decaying; the flow depth remains constant (rather than decreasing) with increasing distance downstream.

Unlike the laminar situation, no analytical method of predicting turbulent velocity profiles is known. Because the vast body of turbulence measurements has been acquired in flows different from the water table (generally either in round pipes or over flat plates), the Newtonian water flow had to be investigated for the water table. (This investigation will serve as a basis for comparison with drag-reducing polymer flows.) As will be shown, the turbulent water-table boundary-layer data are quite similar to turbulent data acquired in more conventional flow geometries. This somewhat surprising result indicates that the limited depth and the presence of a free surface play little or no role. Consequently, the water table should be readily acceptable as a flow device for studying turbulent boundary layers.

Figure 8 shows mean-velocity profiles of several turbulent flows. These data were acquired by each of the three anemometry techniques and closely agree with one

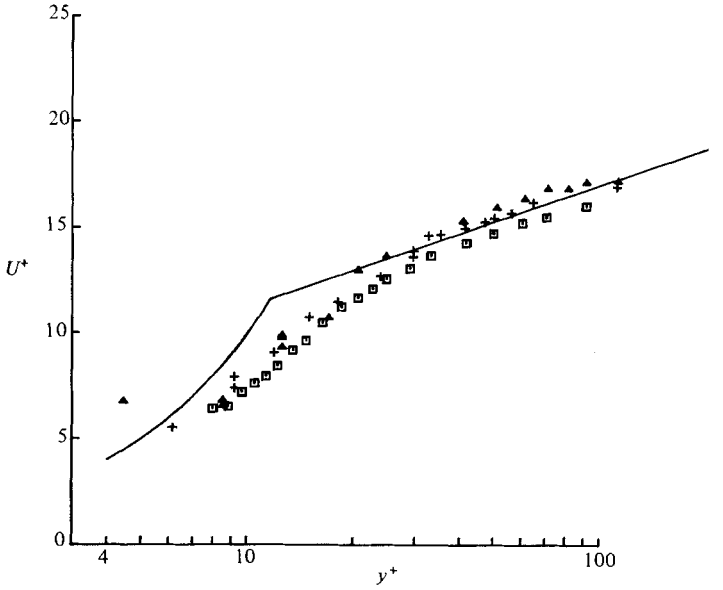

FIGURE 8. Turbulent mean-velocity measurements obtained at $X = 150$ cm: □, hot film; △, selective-seeding LDA; +, uniform-seeding LDA; ——, law of the wall. The scatter about the logarithmic relation is not considered significant.

another. While these flows varied in depth and u_τ, the data fit the law of the wall shown as a solid line. The standard turbulence normalization coordinates have been used, where

$$y^+ = \frac{u_\tau Y}{\nu}, \quad U^+ = \frac{\langle U \rangle}{u_\tau}.$$

The angle brackets denote time averaging.

Turbulent intensity u' profiles are shown in figure 9 for the same flows as figure 8. The intensity, as displayed after normalizing with the wall coordinates, is

$$u'^+ = \frac{\langle (U - \langle U \rangle)^2 \rangle^{\frac{1}{2}}}{u_\tau}.$$

Once again data obtained from the three anemometry techniques are in general agreement. Data of u'^+ published by Ueda & Mizushina (1977) and Ueda & Hinze (1975) are shown by lines on figure 9 to provide comparison with other turbulent flows of limited y^+ extent. These two references were chosen because they also provided skewness measurements. The water-table profiles are qualitatively similar, with u'^+ at a maximum near $y^+ = 15$; however, the value of this maximum is less than that measured by the previously published data. The maximum of u'^+ reached on the water table is 2·3, while it has been generally reported as 2·8 in the literature (Hinze 1978), although some considerable variation has been observed. Coles (1978) reported data from 50 recent publications that dealt with flows in pipes, channels and over flat plates (at zero pressure gradient), and the peak of u'^+ ranged from 2·2 to 3·2. Coles observed no Reynolds-number dependence of this range, but he did note a general trend of the ratio of u'^+ at $y^+ = 50$ to the maximum u'^+ increasing with the y^+ extent of the boundary layer (h^+). At the low Reynolds numbers and boundary-layer thicknesses corresponding to water-table flows ($h^+ \approx 100$), Coles reported this ratio as being about 0·6. The data of figure 9 are in complete agreement with this observation.

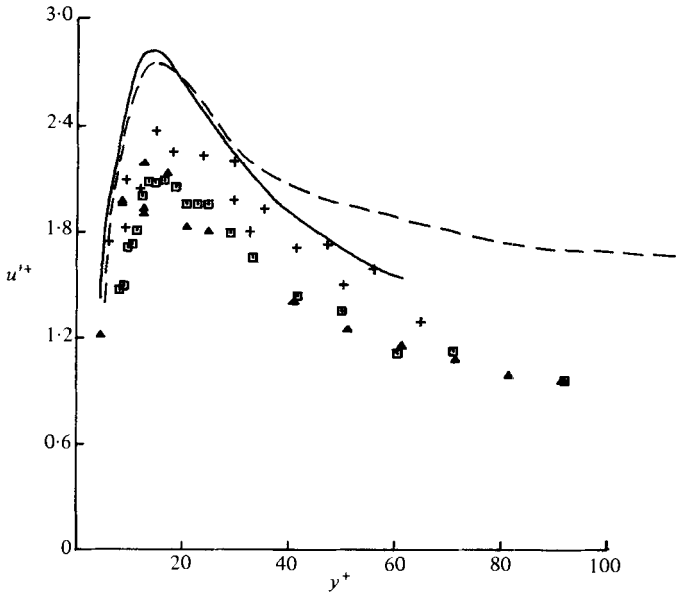

FIGURE 9. Turbulent u'^+ measurements obtained at $X = 150$ cm: □, hot film; △, selective-seeding LDA; +, uniform-seeding LDA; – – –, Ueda & Hinze (1975); ——, Ueda & Mizushina (1977). Differences from the published data are probably significant.

Based on Coles' survey, the u'^+ data fall well within the range of observations made in more-standard flows and should be an acceptable flow in which to study boundary-layer turbulence. Owing to the broad range of previous observations it is difficult to make any statement, although it is suspected that the u'^+ levels are a bit lower than those encountered in pipe flows or flat-plate boundary layers.

Because the water-table flows investigated in this paper are all high-strain-rate flows, the viscous scale is small, which has implications for each of the measuring techniques. The viscous lengthscale ν/u_τ for the flow of figure 11 is only $2{\cdot}38 \times 10^{-3}$ cm; this length is typical of all the flows in the paper. In terms of this length the hot-film sensor is 2·13 lengths in diameter and 42·7 lengths in span; the typical LDA scattering volume (0·11 mm diameter and 1·6 mm length) is then 4·62 lengths in diameter and 67·2 lengths long. When measuring the instantaneous velocity each of the three techniques actually represents a spacial average over one length or other, and therefore each would underestimate u'^+ by an amount which is difficult to determine.

Skewness was relatively unexplored until the advent of digital-computer data analysis. Figure 10 shows skewness profiles for several water-table flows using a normalization similar to that of u'^+, i.e.

$$\mathrm{skw}^+ = \frac{\langle (U - \langle U \rangle)^3 \rangle^{\frac{1}{3}}}{u_\tau}.$$

Traditional statistical normalization based on local u' was considered inappropriate for turbulent boundary-layer measurements, where the measurement of u' might be of questionable accuracy. Data published by Ueda & Mizushina (1977) and Ueda & Hinze (1975) are displayed as lines in figure 10. Qualitatively, the water-table data is quite similar to the other data; the skewness changes sign near $y^+ = 20$, but the overall skewness amplitude is lower than the cited data. This is consistent with the u'^+ comparison with these same references. Literature of skewness measurements is

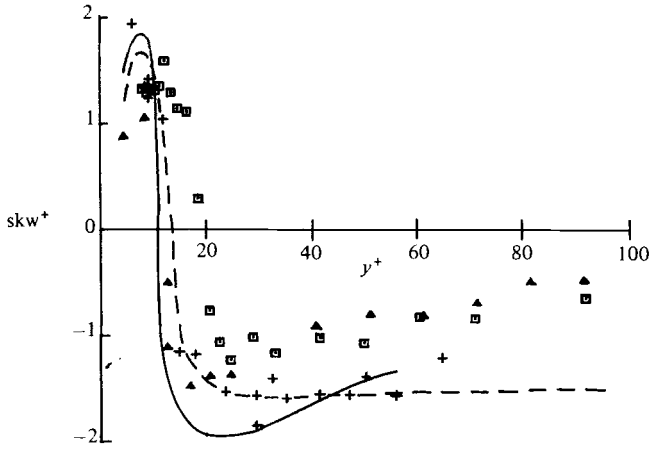

FIGURE 10. Turbulent skewness measurements skw^+ obtained at $X = 150$ cm: □, hot film; △, selective-seeding LDA; +, uniform-seeding LDA; – – –, Ueda & Hinze (1975); ——, Ueda & Mizushina (1977). Differences from the published data are probably significant.

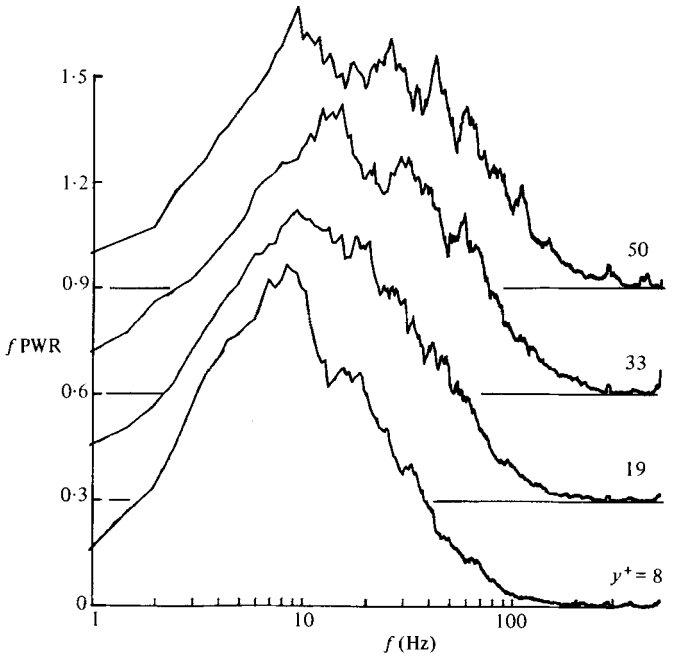

FIGURE 11. Turbulent-velocity spectra obtained at $X = 150$ cm using hot-film anemometry. The visual area under any segment of the curve is directly proportional to the energy at that frequency range. $H = 2{\cdot}91$ mm, $u_\tau = 3{\cdot}67$ cm/s, $\nu = 0{\cdot}875$ cSt.

not yet extensive, but it is likely that the data will be at least as scattered as reported for u'^+ by Coles (1978).

Velocity spectra were also obtained from the digital velocity records and are displayed in figures 11–13. For purposes of clarity the data have been smoothed by displaying at each frequency the average of the local intensity with the other values within ± 5 Hz of the reported frequency. The smoothing is equivalent to a 10 Hz wide ideal filter on the output. Figures 11–13 follow the presentation form used by Morrison & Kronauer (1969), where f PWR is plotted *vs.* $\log f$. The frequency in hertz

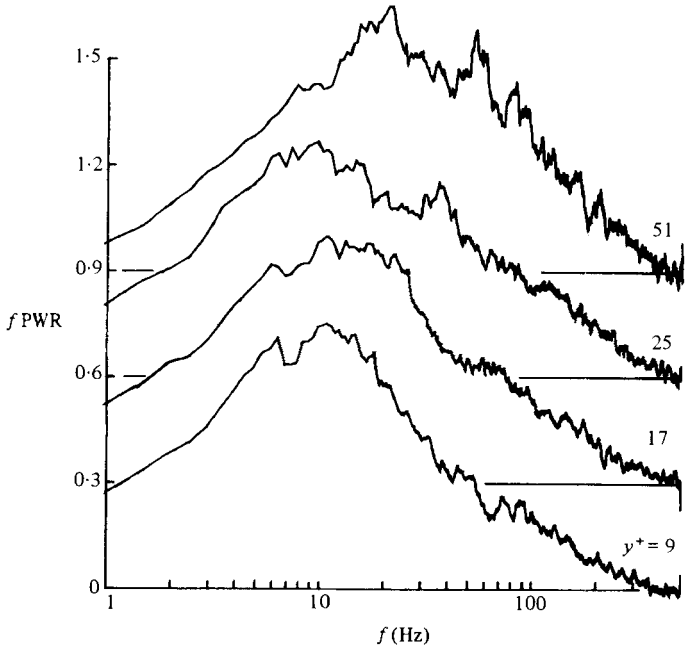

FIGURE 12. Turbulent-velocity spectra obtained at $X = 150$ cm using selective-seeding LDA. $H = 2{\cdot}77$ mm, $u_\tau = 3{\cdot}60$ cm/s, $\nu = 0{\cdot}889$ cSt.

is f, and PWR is the normalized power-spectral density defined in the usual way, namely

$$\text{PWR} = \frac{\Phi}{\ln 10 \int_0^\infty \Phi \, df},$$

where Φ is defined by

$$\Phi = \frac{4\pi^2}{T} a(f)\, a^*(f) - n_{\text{I}}^2 \tag{16}$$

and $a(f)$ is the Fourier transform of the U-velocity (and a^* its complex conjugate), n_{I} is the instrumentation noise (assumed white) and T is the time length of the transformed data record.

The advantage of such coordinates is that one easily recognizes the energy-containing frequencies because the power is directly proportional to the visual magnitude of the area under the curve. The traditional presentation of log PWR *vs.* log f cannot be readily interpreted, while the use of linear axes involves difficulty in including the broad range involved in both Φ and in the frequencies found in turbulent-velocity records. Furthermore, Bullock, Cooper & Abernathy (1978) provide extensive spectra of turbulent air flow in a pipe using this same log f *vs.* f PWR presentation. Their spectra can therefore be used for comparison.

Plotting spectra of f PWR *vs.* log f coordinates has one drawback. There is an implicit assumption that the spectra approach zero faster than $1/f$ at a large frequency. Interpretation is difficult if the data have a significant white-noise component associated with the measuring instrumentation. All LDA is of this character and the noise was eliminated by subtracting an appropriate n_{I} according to (16). The value of n_{I} was selected so that the product f PWR ≈ 0 at high f.

Turbulent spectra are shown in figure 11 using a hot-film sensor to measure velocity. The primary feature to observe is the qualitative similarity of the spectra

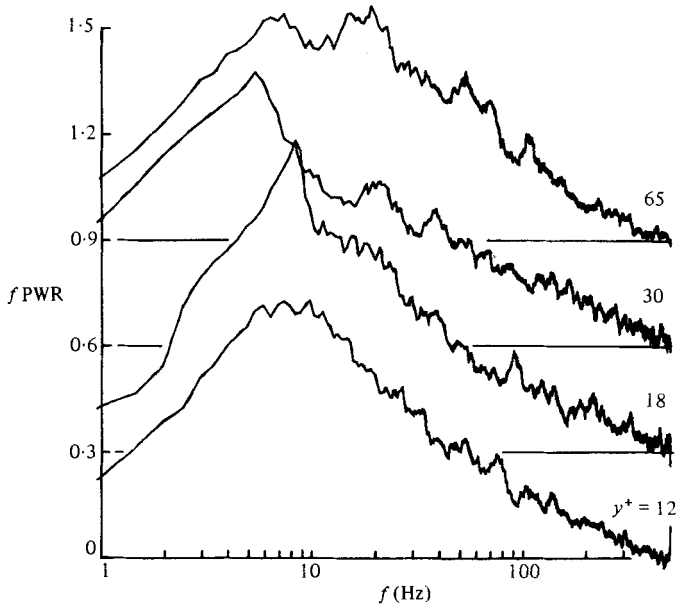

FIGURE 13. Turbulent-velocity spectra obtained at $X = 150$ cm using uniform-seeding LDA. $H = 2{\cdot}93$ mm, $u_\tau = 3{\cdot}46$ cm/s, $\nu = 0{\cdot}901$ cSt.

at the different elevations. The overall form is in general agreement with the air data of Bullock *et al.* (1978). They found a peak of the spectrum near the wall at $f^+ = 0{\cdot}0069$, where $f^+ = fv/u_\tau^2$, while the water-table data have a peak between 0·005 and 0·009. The water-table spectra do not appear to collapse onto a single curve if one uses the wall parameters to non-dimensionalize.

Spectra obtained using the selective seeding LDA are displayed in figure 12. Although adjustment was made to bring the high-frequency points down to the axis (to eliminate the white-noise content of the data), some difference from the hot-film data persists. If the noise had the form of a low-pass-filtered white spectrum, the hot-film data could be replicated precisely. Lacking any reasonable procedure for doing this, nothing was done to improve the LDA spectra other than a uniform n_1 subtraction to bring the highest-frequency data down to the axis. Noise levels found for the transformed data were about the same as those for the u'^+ data, using a completely different criterion.

Figure 13 shows spectra obtained using uniform-seeding LDA for another flow. There is no significant change from the data presented in figures 11 and 12 due to either the flow or the anemometry device. As with selective seeding, there is an increased noise level with the uniform-seeding LDA compared with hot-film measurements.

One last set of measurements were taken to confirm the turbulent nature of a tripped water-table flow. Sodium sulphate crystals sprinkled into the flow provided a simple way of measuring the streak spacing. This method determined $\lambda^+ \approx 116 \pm 15$, in close agreement with the generally accepted streak spacing of $\lambda^+ = 100$ (Hinze 1978).

6. Conclusions

The flow of water on a water table has been described in detail, and the facility has been demonstrated to be a useful tool for studying laminar and turbulent boundary layers. The free surface provides excellent flow visualization. Two laser-Doppler anemometry techniques obtaining nearly continuous velocity data at strain rates above those needed for onset of polymer drag reduction have been demonstrated as effective in pure-water flows. These techniques have been compared with measurements obtained using hot-film sensors for verification.

Laminar boundary layers generated on the water table can be modelled mathematically, and the comparison of the predicted flow depth and velocity profiles with measurements as a function of streamwise distance down the table is excellent. At a fixed flow rate the Reynolds number based on average velocity and local flow depth is constant, while the wall strain rate increases in the streamwise direction. Surface tension is not important in determining the mean flow.

Turbulent boundary-layer flows, generated by introducing a three-dimensional disturbance across the entire water-table inlet, show all the features of turbulent boundary layers generated in more-standard apparatus. Mean velocity profiles follow the law of the wall, u'^{+} has a maximum near $y^{+} = 15$, skewness changes sign in the range of $y^{+} = 20$, and velocity spectra are similar in form to those in the published literature. The fact that this flow is of very limited y^{+} extent apparently causes no significant change in U-velocity information.

The financial support of NSF (CME 79-05960) is gratefully acknowledged, as is that of the Division of Applied Sciences at Harvard University.

REFERENCES

ABERNATHY, F. H., BERTSCHY, J. R. & CHIN, R. W. 1977 Turbulence spectra using laser-Doppler anemometry and selective seeding. In *Proc. 5th Biennial Symp. on Turbulence, Missouri-Rolla, Paper* P.S. 13.

ABERNATHY, F. H., BERTSCHY, J. R., CHIN, R. W. & KEYES, D. E. 1980 Polymer induced fluctuations in high strain laminar flows. *J. Rheol.* **24**, 647–665.

BERTSCHY, J. R. 1979 Laminar and turbulent boundary layer flows of drag-reducing solutions. Ph.D. thesis, Division of Applied Sciences, Harvard University.

BERTSCHY, J. R. & ABERNATHY, F. H. 1977 Modifications to laminar and turbulent boundary layers due to the addition of dilute polymer solutions. In *Proc. 2nd Int. Conf. on Drag Reduction, BHRA Fluid Engineering, Paper* G1.

BERTSCHY, J. R. & ABERNATHY, F. H. 1981 Novel method of traversing a forward scatter laser-Doppler anemometer. *Rev. Sci. Instrum.* **52**, 1013–1015.

BRUIN, G. J. DE 1974 Stability of a layer of liquid flowing down an inclined plane. *J. Engng Math.* **8**, 259–270.

BULLOCK, K. J., COOPER, R. E. & ABERNATHY, F. H. 1978 Structural similarity in radial correlations and spectra of longitudinal velocity fluctuations in pipe flow. *J. Fluid Mech.* **88**, 585–608.

COLES, D. 1978 A model for flow in the viscous sublayer. In *Proc. Workshop on Coherent Structure of Turbulent Boundary Layers, Lehigh University.*

EMMONS, H. W. 1951 The laminar–turbulent transition in a boundary layer – Part I. *J. Aero. Sci.* **18**, 490–498.

HANSEN, R. J., LITTLE, R. C., REISCHMAN, M. M. & KELLEHER, M. D. 1974 Stability and the laminar to turbulent transition in the pipe flows of drag reducing polymer solutions. In *Proc. 1st Int. Conf. on Drag Reduction, BHRA Fluid Engineering, Paper* B4.

HINZE, J. O. 1978 *Turbulence*, 2nd edn. McGraw-Hill.

JONES, W. M., MARSHALL, D. E. & WALKER, P. C. 1976 The flow of dilute aqueous solutions of macromolecules in various geometries: II. Straight pipes of circular cross-section. *J. Phys.* D (*Appl. Phys.*) **9**, 735–752.

LIN, S. P. 1967 Instability of a liquid film flowing down an inclined plane. *Phys. Fluids* **10**, 308–313.

MISES, R. VON 1927 Bemerkungen zur Hydrodynamik. *Z. angew. Math. Mech.* **7**, 425–431.

MITCHELL, A. R. & THOMSON, J. Y. 1958 Finite difference methods of the solutions of the von Mises boundary layer equation with special reference to conditions near a singularity. *Z. angew. Math. Phys.* **9**, 26–37.

MORRISON, W. R. B. & KRONAUER, R. E. 1969 Structural similarity for fully developed turbulence in smooth tubes. *J. Fluid Mech.* **39**, 117–141.

UEDA, H. & HINZE, J. O. 1975 Fine-structure turbulence in the wall region of a turbulent boundary layer. *J. Fluid Mech.* **67**, 125–143.

UEDA, H. & MIZUSHINA, T. 1977 Turbulence structure in the inner part of the wall region in a fully developed turbulent tube flow. In *Proc. 5th Biennial Symp. on Turbulence, Missouri-Rolla, Paper* V.4.

YIH, C. S. 1963 Stability of liquid flow down an inclined plane. *Phys. Fluids* **6**, 321–334.